High-performance X-ray detectors for the new powder diffraction beamline I11 at Diamond

Nicola Tartoni,[a] Stephen P. Thompson,[a]* Chiu C. Tang,[a] Brian L. Willis,[a] Gareth E. Derbyshire,[a,b] Anthony G. Wright,[c] Stephen C. Jaye,[c] J. Michael Homer,[c] John D. Pizzey[c] and Anthony M. T. Bell[d]

[a]Diamond Light Source, Diamond House, Chilton, Didcot, Oxon OX11 0DE, UK, [b]STFC Rutherford Appleton Laboratory, Chilton, Didcot, Oxon OX11 0DE, UK, [c]Sens-Tech Ltd, Bury Street, Ruislip, Middlesex HA4 7TA, UK, and [d]STFC Daresbury Laboratory, Warrington WA4 4AD, UK. E-mail: stephen.thompson@diamond.ac.uk

The design and performance characterization of a new light-weight and compact X-ray scintillation detector is presented. The detectors are intended for use on the new I11 powder diffraction beamline at the third-generation Diamond synchrotron facility where X-ray beams of high photon brightness are generated by insertion devices. The performance characteristics of these detection units were measured first using a radioactive source (efficiency of detection and background count rate) and then synchrotron X-rays (peak stability, light yield linearity and response consistency). Here, the results obtained from these tests are reported, and the suitability of the design for the Diamond powder beamline is demonstrated by presenting diffraction data obtained from a silicon powder standard using a prototype multicrystal analyser stage.

Keywords: X-rays; X-ray diffraction; detectors; beamlines.

1. Introduction

Modern third-generation synchrotron radiation facilities provide photon beams that combine extremely high photon fluxes with very high collimation. This not only opens up the possibility of new research fields but also offers the opportunity to make significant advances in the quality and nature of data obtainable from established techniques such as X-ray powder diffraction. Although existing off-the-shelf detector systems have advanced, they are in the main still unable to handle the enormous photon rates produced by modern insertion devices such as wigglers, undulators or free-electron lasers.

The quality of data obtained from measurements involving X-rays depends directly upon the nature of the detector being used. A detector with a high background leads to a loss of information carried in weak signals, while a detector with a low saturation level severely limits both the type of experiment and the level of information that can be extracted from it. Except in the simplest of diffraction experiments, for example, where only the positions of the strongest peaks may be required, it is vital to employ a detector with as large a dynamic range as possible. Although an attenuator can be placed before the detector to reduce the photon rate, this in effect wastes much of the power of modern light sources. Detector performance is therefore a limiting factor in realising state-of-the-art beamline designs.

To overcome the disparity between source characteristics and detector performance thus requires either the improvement of existing detector concepts or the introduction of new approaches. Early on, two types of counting detector were commonly used for X-rays in the energy region 5–40 keV, the NaI-based scintillation detector and the gas-filled diode (proportional) detector (see Knoll, 2000 or Cullity & Stock, 2001 for general reviews). Both are, in principle, capable of handling count rates in excess of 1×10^6 counts s^{-1} with low backgrounds. However, gas-filled proportional detectors suffer from ageing effects limiting their useful life times, while NaI scintillators, though possessing a high light output level compared with many other scintillation materials, have a long pulse decay constant of 230 ns. Since photomultiplier tubes (PMTs) have response times of typically less than ∼10 ns, the scintillator decay rate was the limiting factor in the maximum theoretical count rate of early detectors. During the 1990s, yttrium aluminium perovskite activated by cerium, YAlO$_3$:Ce, commonly abbreviated to YAP(Ce), scintillators were produced with a light pulse decay time of ∼27 ns (Cockerton et al., 1995). The limiting factor in determining the maximum count rate then became the electronics associated with processing the PMT signal and in particular the requirement for a suitable amplifier capable of shaping pulses with sufficiently narrow widths (Harada et al., 2001). In order to ensure there is no ballistic deficit, good pulse-shaping for high-count-rate applications is three to four times the scintillation decay

time, τ. Even higher rates can in principle be achieved using shorter shaping times of one to two times τ, but these result in poorer pulse-height resolution. The ideal pulse width for YAP(Ce) is thus $\sim$90 ns, whereas conventional scintillation detector amplifiers could only shape much wider pulses of 3–30 µs. Commercially produced detectors based on YAP(Ce) crystals are now available, but do not appear to be optimized for high count rates, typically managing $\sim$2.5 $\times$ 10^6 counts s^{-1}. Although this may meet some application requirements, bespoke detectors are often still required. For example, Harada *et al.* (2001) reported a detector capable of 5 $\times$ 10^6 counts s^{-1} with 16.5 keV X-rays, while more recently Kishimoto & Yamamoto (2003) produced a detector giving >5 $\times$ 10^6 counts s^{-1} for X-rays in the range 16.6–50 keV.

In this paper we describe the design and performance characteristics of a new compact light-weight X-ray detector based on a YAP(Ce) scintillator–PMT combination coupled to a new hardware-based approach to signal processing. Developed initially for use with a prototype multiple analysing crystal (pMAC) system for the powder diffraction beamline I11 at Diamond, the detector has the potential of deployment on other Diamond beamlines, *e.g.* I15 (Extreme Conditions). This paper is one of a series of papers detailing the new design concepts and instrumentation underpinning the new powder diffraction beamline.

1.1. Overview of beamline I11

Currently under construction and due to complete in August 2008 (target date), beamline I11 will be sourced by a 90-pole in-vacuum undulator located within a straight section of the 3 GeV electron storage ring. This will deliver high-intensity monochromatic X-rays over the 5–30 keV range to a small sample area (1 mm $\times$ 5 mm). A full description of the beamline design has been given by Tang *et al.* (2008) outlining the main optical components. Briefly, these principally comprise a cryogenically cooled double-crystal (Si 111) monochromator and a double-bounce harmonic rejection mirror assembly. These will produce a high-purity parallel X-ray beam of 0.8 mm (vertical) by 5 mm (horizontal) [full width at half-maximum (FWHM)] at the sample position, located at the centre of a new heavy-duty diffractometer. Typical photon flux at 10 keV will be of the order of 10^{14} photons s^{-1} mm^{-2} (0.1% bandpass)$^{-1}$. The optical components are housed in a separate optics hutch with only monochromatic radiation being delivered, *via* transfer line, to the experimental hutch which houses the diffractometer and final beam conditioning and diagnostic components (slits, I_0 monitor *etc.*). The main performance specifications of the I11 beamline are listed in Table 1.

2. Multiple analysing crystal stages and detector requirements

Analyser stages, owing to the inherently narrow rocking curves of their constituent low bandpass (LBP) Si or Ge crystals which thus provide for tight angular collimation, offer

Table 1
Performance specifications of beamline I11 at Diamond.

Resolution, stability, divergence and X-ray flux cited for an operational energy of 10 keV and 300 mA electron beam current.

Requirement	Specification
Energy range	5–30 keV (0.4–2.4 Å)
Energy resolution ($\Delta E/E$)	1.5 $\times$ 10^{-4}
Energy stability	<0.5 eV
Beam divergence	30 µrad (V) $\times$ 100 µrad (H) (FWHM)
X-ray flux at sample	10^{14} photons mm^{-2} s^{-1} (0.1% bandpass)$^{-1}$

the highest possible resolution currently available for powder diffraction measurements (see reviews by Cox, 1991, 1992). However, owing to the inherent loss of intensity associated with their use (and a consequent increase in the time needed to collect data with good signal to noise), their routine deployment on powder diffractometers has only really become viable at third-generation sources. Furthermore, to fully exploit the high angular resolution offered by analyser crystals, the angular step size between adjacent points in 2θ must be reduced to a few mdeg per step, further increasing both the total number of data points collected and the time required to record an entire powder pattern, both of which are detrimental to beam-time efficiency and user throughput (though improvements are possible if step-wise scanning is replaced by continuous scanning, whereby data collection times are limited by the speed of the diffractometer movement irrespective of the frequency of the data points). To overcome these limitations, early analyser designs adopted a multicrystal approach (Hodeau *et al.*, 1998). This essentially replaced the single angle-stepping slit detector, or crystal detector, arrangement of traditional diffractometers with a stacked array of LBP analysing crystals and detectors, which for n crystals provided n whole diffraction patterns for the time cost of a single scan in 2θ and a new generation of powder diffraction beamlines based on this design were successfully commissioned (Gozzo *et al.*, 2004; Fitch, 2004).

For beamline I11, a new approach involving multi-analysing crystal stages (Tang *et al.*, 2008) has been adopted to both further advance analyser technology and to ensure the provision of a state-of-the-art powder facility at Diamond. Fig. 1 shows schematically the I11 multi-MAC arrangement. In this design the diffracted radiation from the sample is analysed by up to 45 flat Si 111 single crystals, but, to provide for fast data collection times by minimizing the angular range over which the instrument's 2θ circle must move, these are arranged on five independent rotation stages distributed around the instrument's 2θ circle. Each stage thus comprises nine crystals offset from each other by 2°, with each crystal having its own dedicated detector (Fig. 2). Although the drawing presented is for a downward scattering geometry, the design also works with upward scattering geometry. The available space between adjacent detector positions amounts to only 27 mm and necessitates a compact housing design. In brief, each analyser stage scans through a small portion (18° 2θ) of the total diffraction pattern, with the final full powder pattern being constructed piecemeal from the patterns recorded by each of
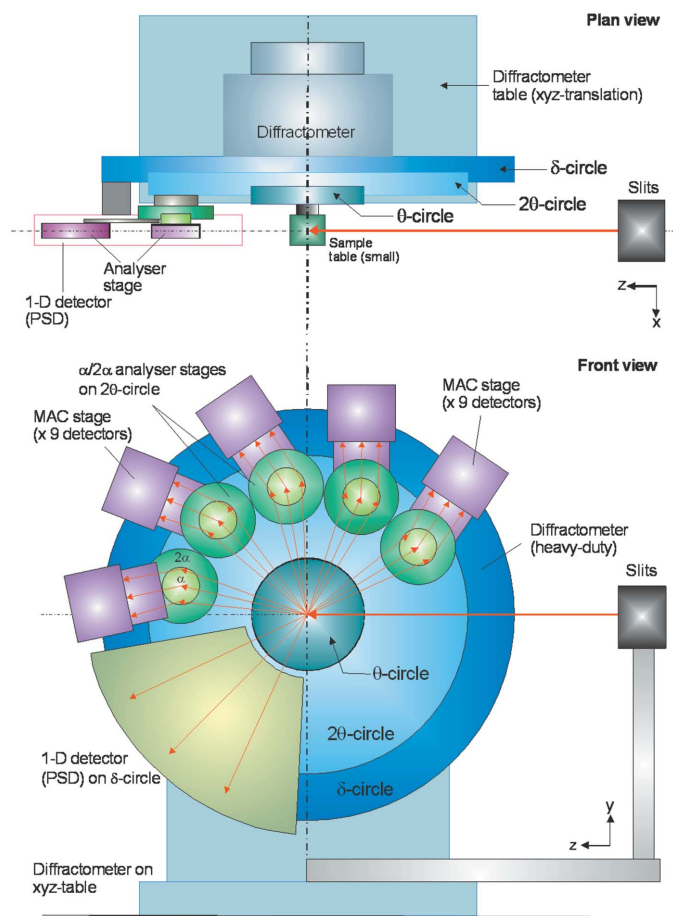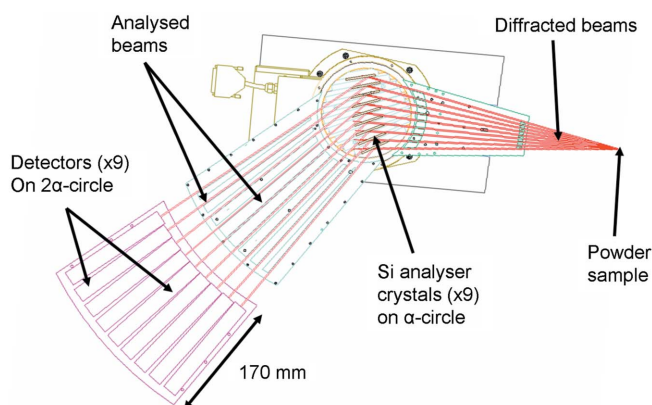
Figure 1
Schematic representation of the beamline I11 multi-MAC stages distributed around the diffractometer 2θ circle. The direction of the X-ray beam is shown right to left.
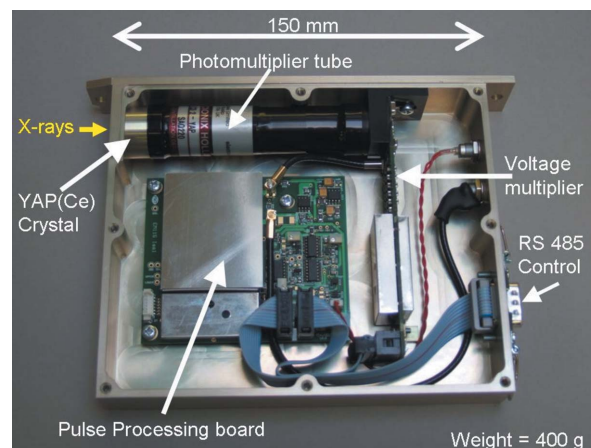

Figure 2
Detailed drawing of a single MAC stage showing the location and the analyser–detector (×9) arrangement.

(vi) Maximum weight of 500 g.

(vii) Uniformity of performance across all 45 units.

Based on these requirements, three prototype units were produced by Electron Tubes Ltd (now Sens-Tech Ltd). These Diamond Electron Tubes X-ray (DELT-X) detectors were used as the basis of the performance and characterization work reported here.
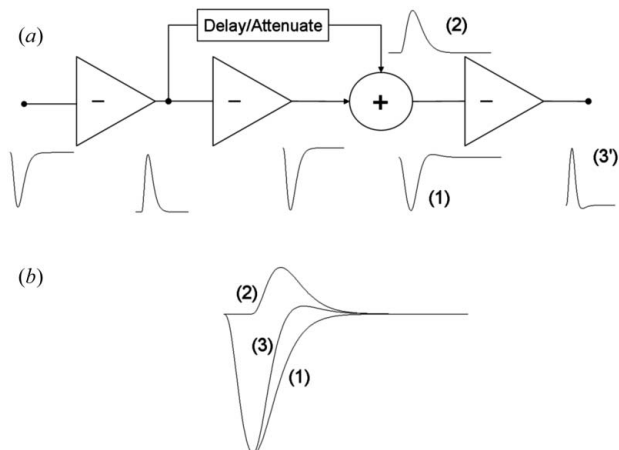
3. Detector details

Fig. 3 shows a DELT-X unit with side lid removed and its main components labelled: 2 mm thick YAP(Ce) scintillation crystal, photomultiplier tube (PMT), voltage multiplier (VM) board and pulse processing (PP) board. The electronic components have been specifically designed to meet the requirements listed above. The VM board supplies high voltages to dynodes in the PMT. These are biased through an active network in order to minimize the difference in voltage between instances when the PMT delivers low and high currents in order to maintain inter-dynode potentials regardless of the mean anode current drawn by the PMT. The PP

the five stages. In practice each stage produces nine individual patterns that are corrected for the crystal offsets and summed to give a single pattern for each stage. The deployment of 45 such detectors across each of the five stages around the 2θ circle therefore also carries with it a stringent requirement for a high degree of uniformity of performance. Because the bulk of the weight of each analyser lies in the two-motor concentric rotation stage that supports both the analyser crystals and detectors, in order not to upset the balancing of the 2θ circle the total weight of each individual detector unit must be less than 500 g.

The key design constraints imposed on the detector from the beamline design, powder diffraction requirements and analyser stage design may be summarized as follows.

(i) Operational energy range of 5–30 keV, with over 95% of impinging photons interacting with the sensitive volume.

(ii) Maximum count rate of at least 5×10^6 counts s^{-1}.

(iii) Maximum background count rate of 0.15 counts s^{-1} in a radiation screened environment.

(iv) Active area for each detector of 15 mm diameter.

(v) Overall housing dimensions for each detector unit of 150 mm (length) × 25 mm (width) × 128 mm (height).
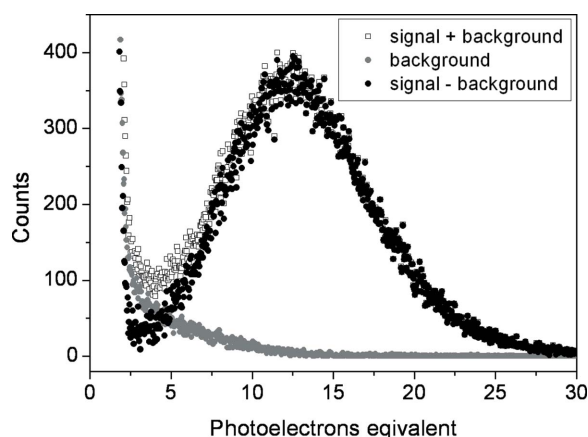

Figure 3
Photograph of a DELT-X unit with side lid removed revealing the major components of the detector system.

board contains an amplifier followed by a discriminator which gives an LVDS logical signal output. Fig. 4 shows a block diagram of the PP board pulse-shaping process. After the first amplification stage the signal from the PMT anode is sent down two separate paths. In one the signal is inverted by a buffer stage, while in the other the signal is both delayed and attenuated. The signals from the two paths are then recombined and the resulting summed signal sent to the discriminator. The measured dead-time is 80 ns using a paralyzable model (Knoll, 2000). Both VM and PP boards have a common RS485 interface to allow remote setting of the voltage parameters (PMT bias voltage, discriminator threshold and window height) by the data acquisition system. This is essential, since their optimum values vary according to the X-ray energy used in any given experiment and will be set automatically without user intervention. For diagnostic purposes the anodic current is also available through a buffer stage and Lemo coaxial connector. Each unit has a compact housing (25 mm × 128 mm × 150 mm) and is light-weight (400 g), thus meeting the space and weight requirements.

The detectors were first tested at the factory using a radioactive source and commercial MCA. The YAP(Ce) crystal gives 12 photoelectrons for the peak of the ^{55}Fe spectrum as shown in Fig. 5. Analysis of this spectrum shows that 59% of the events appear to the right of the peak, i.e. the efficiency of detection if the threshold is set to 5.9 keV. At twice the energy of the dominant emission line and with the lower threshold still set at 5.9 keV, 96% of events are counted above a threshold >6 photoelectrons. The devices were also shielded with lead blocks and tested for intrinsic electronic background. All three met the specified requirement of 0.15 counts s^{-1}.

4. Synchrotron X-ray detection

The prototype detectors were tested on the powder diffraction station 2.3 at the Synchrotron Radiation Source (SRS), Daresbury Laboratory. Fig. 6 shows a photograph taken with the DELT-X detectors mounted on the pMAC stage mounted on the 2.3 powder diffractometer. This instrument, located 15 m from a 1.2 T dipole bending magnet, is a concentric two-circle (θ, 2θ) high-resolution angle-scanning diffractometer, based on a parallel-beam optics design. It receives X-rays in the range 0.5–2.5 Å, with monochromatic beam being selected via a water-cooled Si 111 channel-cut single crystal. This delivers a parallel beam of $\sim$15 mm (H) by 1.8 mm (V) with $\sim$10^9 photons mm^{-2} (0.1% bandwidth)$^{-1}$, for a 200 mA electron beam current at 10 keV, to the sample stage located at the centre of the instrument's two circles. Technical details of the beamline are described by Collins et al. (1992). Wavelength, or energy, calibration of the monochromator was performed using a high-purity Si powder standard (SRM640c) from the National Institute of Standards and Technology and an automated fitting procedure to the Si powder peak positions (Laundy et al., 2003). For the purpose of the tests, air scatter along the primary beam path was used to give the

Figure 4
Schematic block diagram of the signal pulse train through the DELT-X pulse-processing board: (a) the logic circuit showing the pulse shape at each step and (b) the result of combining the inverted pulse (1) with the delayed and attenuated pulse (2) to produce a narrower pulse profile (3) which is then inverted for output (3′).
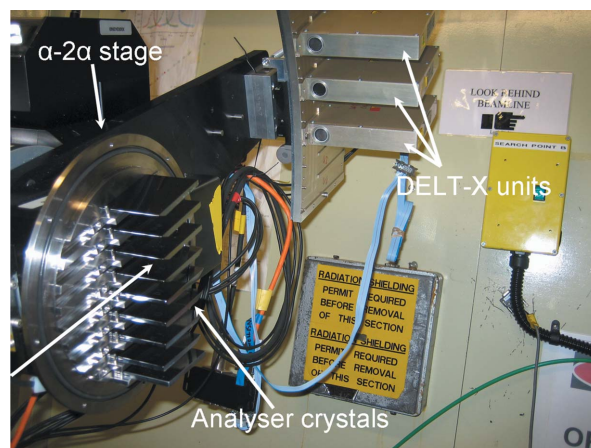
Figure 5
Typical detector efficiency and background spectrum of the YAP(Ce) crystal obtained from the ^{55}Fe source.

Figure 6
Three DELT-X detectors on the pMAC mounted on the station 2.3 powder diffractometer. The white arrow indicates the approximate direction of the beam.

required high count rates, *i.e.* with no scattering sample at the sample position and analyser crystals removed. The detector modules were positioned at suitable 2α and 2θ angles above the primary beam so as to give the desired count rates at any given energy. In this configuration three basic characterizations were performed. The first was to assess the peak stability as a function of count rate; the second addressed the linearity of the light yield of the YAP(Ce) crystal, while the third checked the consistency of the detector response as a function of PMT amplification.

5. Results and performance

5.1. Peak stability

At a fixed energy of 10 keV and various fixed detector positions (for different count rates), the PMT bias voltage was set to 800 V, the upper discriminator window level to 4000 mV and the lower discriminator window (pulse height) step-scanned from 25 to 3500 mV in 25 mV steps. At each step the counting time was set for between one and a few seconds dependent on the statistics. Fig. 7 (main plot) shows the results of this test and shows the first derivative ($\mathrm{d}N/\mathrm{d}V$) as a function of pulse height (PH) for various count rates (inserted plot). As indicated by the arrow in the inset figure, the minimum points all occur at approximately the same place (365 ± 25 mV), which allows for a reliable setting of the threshold during operations. The peak positions are sufficiently well away from the pedestal peak present at low threshold values. These features and response characteristics indicate that the detector is functioning as intended. Note that the measured count rate has been corrected for dead-time using a paralyzable model,

$$R_{\mathrm{obs}} = R_{\mathrm{cor}} \exp\left[-R_{\mathrm{cor}}\tau\right], \tag{1}$$

where R_{obs} is the observed count rate, R_{cor} is the dead-time-corrected count rate and τ is the dead-time (80 ns).
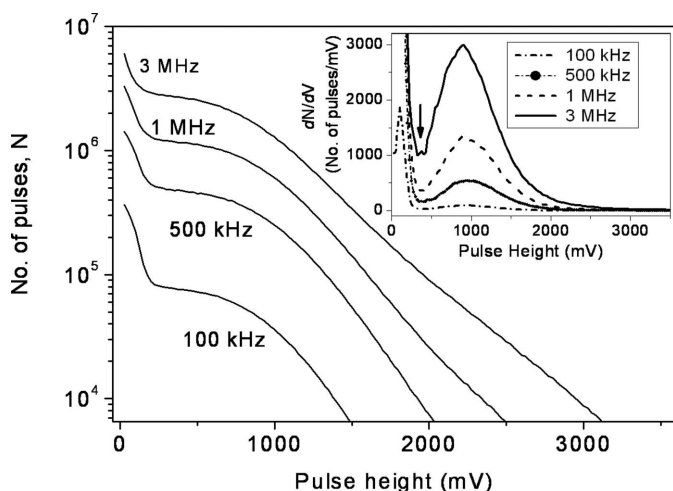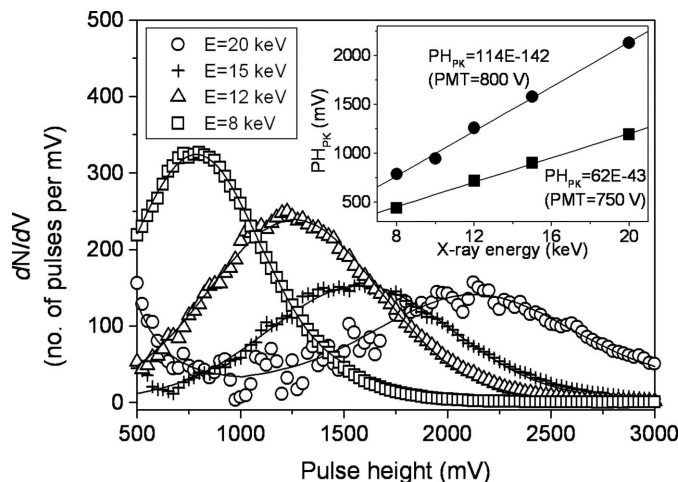
5.2. Light yield linearity

The step-wise scans above were repeated at 8, 12, 15 and 20 keV and the $\mathrm{d}N/\mathrm{d}V$ curves are shown in Fig. 8. For each energy the peak position of the pulse height ($\mathrm{PH_{PK}}$) was extracted by fitting the data with a Gaussian function and the results plotted as a function of energy (Fig. 8, inset, top right). As can be seen, the light yield of the YAP(Ce) crystal shows excellent linearity across the energy range investigated. Although we could not probe the lower (5 keV) and upper 20–30 keV range, owing to the limitations of station 2.3, we are confident that this linearity will extend across the whole I11 spectrum since, for a PMT bias of 800 V, it is governed by

$$\mathrm{PH_{PK}} = 114E - 142, \tag{2}$$

where the peak position is in mV and E in keV. We also tested the pulse-height response with different gains, *i.e.* PMT voltages of 700, 750 and 850 V. With these settings the resulting heights of the pulses span a wide dynamic range of the amplifier-shaper without becoming saturated. Similar linear E–$\mathrm{PH_{PK}}$ dependencies were observed, *e.g.* for 750 V (Fig. 8 insert, lower data set). The corresponding equations determined for each voltage and stated on the plots will be used to automatically select the correct settings of threshold and window voltages during beamline operation.

5.3. Consistency of detector response

For a normal detector the total count rate should be constant over a range of PMT voltages, *i.e.* by changing the gain the integrated pulses should be the same. We put DELT-X to the test by measuring the response at 700, 750, 800 and 850 V with a moderate count rate of 200–300 kHz. The results are shown in Fig. 9(a); the main plot shows the number of pulses measured by scanning the lower window voltage as before. The plot of $\mathrm{d}N/\mathrm{d}V$ as a function of PH (inserted plot) shows that the peak centre is systematically shifted away from

Figure 7
The response characteristic of the DELT-X detector measured at 10 keV with PMT = 800 V and various count rates (main plot). The $\mathrm{d}N/\mathrm{d}V$ derivative with respect to pulse height is presented (inset) with the point of minimum ($\sim$365 mV) indicated by the arrow.

Figure 8
The $\mathrm{d}N/\mathrm{d}V$ derivative as a function of PH measured at various energies with PMT = 800 V (main plot). For clarity, the curve for $E = 10$ keV is omitted. The solid lines are the corresponding fits using a Gaussian function. The peak positions ($\mathrm{PH_{PK}}$) obtained are plotted as a function of energy for PMT = 750 and 800 V (inset).
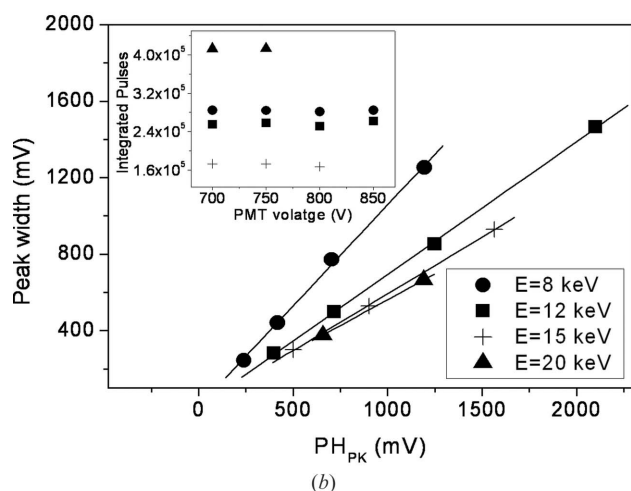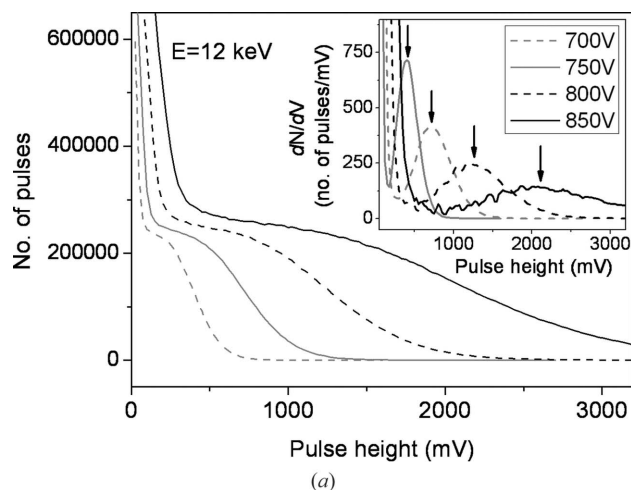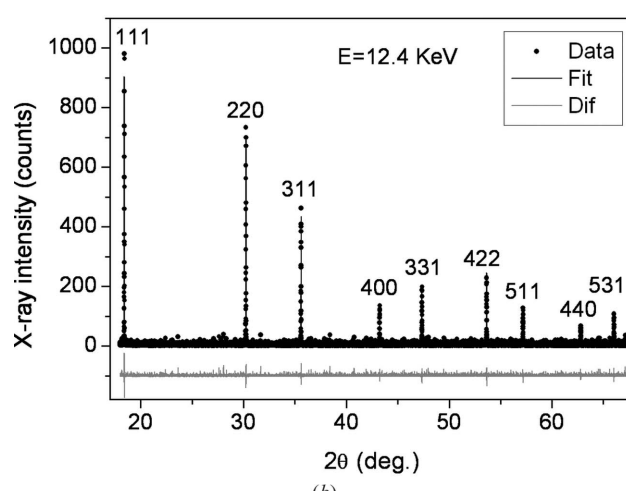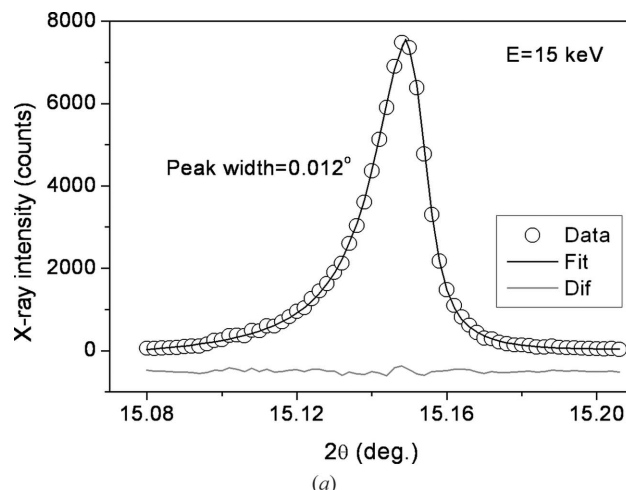
Figure 9
(a) The response characteristic measured with different PMT voltages using an X-ray beam of 12 keV. The dN/dV derivative as a function of PH (inserted plot) illustrates the systematic shift of the peak position (PH_{PK}) with bias voltage as shown by the arrows. (b) The linear relationship between PH_{PK} and peak width (FWHM) obtained at various energies (main graph). The integration of N, observed at operational bias voltages (insert plot), shows 'uniformity' response of the DELT-X device.

Figure 10
(a) Silicon powder peak measured using a single analyser–detector pair with an X-ray beam of 15 keV. The solid line is the fitted curve using a pseudo-Voigt function and the difference between the experimental and fitted data is shown by the lower trace. (b) Silicon powder pattern obtained with an X-ray beam of 12.4 keV. The experimental data (points) were fitted using known structural details and experimental parameters.

the pedestal with increasing bias voltage. In addition, the width of the peak increases with the gain. From further analysis of fitting the peak at each PMT setting with a Gaussian function (excluding the data below the minimum point), the FWHM and PH_{PK} were extracted (Fig. 9b). Again, the behaviour at the energies investigated shows a linear relationship which in turn indicates that the integrated areas are constant as concluded in Fig. 9(b) (inset). The results from these measurements clearly demonstrate that the detector both responds and functions according to specification.

6. Powder diffraction

As an application example of the suitability of the DELT-X units for deployment on the I11 diffractometer MAC stages, Fig. 10(a) shows a diffraction peak collected by scanning the pMAC stage through the 2θ angular range containing the diffracted signal from the silicon 111 powder reflection. The

sample was held in a small spinning glass capillary (0.5 mm diameter) at the diffractometer centre and irradiated by an X-ray beam of 15 keV. This diffraction geometry is one of the standard set-ups on this beamline (MacLean et al., 2000). The data presented were obtained from a single analyser–detector pair with a fine scan step of 0.002° s^{-1}. Note that the narrow peak width is due to the powder particle size/strain effect, while the peak asymmetry is due to the well known geometric effect of axial divergence. The peak shape could be readily described using a pseudo-Voigt function as shown by the excellent fit. The fitting was performed using TOPAS (Bruker, Version 2.1) which is a software package for general profile and structure analysis of powder diffraction data. As these DELT-X units are designed and built for powder diffraction experiments which usually involve the collection of an entire pattern, it was therefore necessary to also collect data over a wide angular range as our final test of the design. Using the same sample specimen and experimental configuration, a whole powder pattern using a scan step of 0.02° s^{-1} was

collected (Fig. 10*b*). To improve the data statistics and angular resolution, a finer step with longer counting time would normally be used to compensate for the relatively low flux on this beamline, but was not possible owing to the limitations of beam-time allocation. Nevertheless, the pattern obtained has been fitted (*i.e.* refined) successfully using standard analytical methods starting from the known structural details of silicon and the instrumental parameters. The fitted data are also shown in Fig. 10(*b*).

7. Conclusions

We have developed new compact and light-weight detectors, DELT-X. Although less efficient, the detection of low-energy X-rays (6 keV) will be possible as shown by the results obtained from the ^{55}Fe source. To ensure parity between measurements, a single device was used for the functional and performance tests using synchrotron X-rays on station 2.3 at the SRS. The DELT-X unit performed satisfactorily with the illumination of low, moderate and high photon intensity for a range of X-ray energies from 6 to 20 keV. We have also examined the responses at different gains (PMT bias voltages) with different photon energies. The observed characteristics led us to conclude that the detector design can be used to reliably register correct X-ray signal strengths. Having established this, the next logical step was the collection of powder data which was demonstrated by the measurement of a whole Si powder pattern. Analysis of the diffraction data using standard techniques showed that the X-ray pattern can be described using known structural information for Si, as expected. Owing to the success of the DELT-X detector development and testing programme, their use in multiple multi-analyser stages will represent a significant step forward in the design of a new generation of powder diffractometers based on the I11 concept, as well as on other state-of-the-art beamlines. As for beamline I11, these detectors will be deployed on the instrument's multiple MAC stages, providing a fully functioning state-of-the-art high-resolution powder diffraction facility on day 1 of user operations.

References

Cockerton, S., Tanner, B. K. & Derbyshire, G. (1995). *Nucl. Instrum. Methods Phys. Res. B*, **97**, 561–566.
Collins, S. P., Cernik, R. J., Pattison, P., Bell, A. M. T. & Fitch, A. N. (1992). *Rev. Sci. Instrum.* **63**, 1013–1014.
Cox, D. (1991). *Handbook on Synchrotron Radiation*, Vol. 3, edited by G. S. Brown & D. E. Moncton, p. 155. Amsterdam: Elsevier Science.
Cox, D. (1992). *Synchrotron Radiation Crystallography*, edited by P. Coppens, p. 186. London: Academic Press.
Cullity, B. D. & Stock, S. R. (2001). *Elements of X-ray Diffraction*, 3rd ed. London: Prentice Hall International.
Fitch, A. N. (2004). *J. Res. NIST*, **109**, 133–142.
Gozzo, F., Schmitt, B., Bortolamedi, Th., Giannini, C., Guagliardi, A., Maden, D., Willmott, P. & Patterson, B. D. (2004). *J. Alloys Compd.* **362**, 206–217.
Harada, M., Sakurai, K., Saitoh, K. & Kishimoto, S. (2001). *Rev. Sci. Instrum.* **72**, 4308–4311.
Hodeau, J. L., Bordet, P., Anne, M., Prat, A., Fitch, A. N., Dooryhée, E., Vaughan, G. & Freund, A. (1998). *Proc. SPIE*, **3448**, 353–361.
Kishimoto, S. & Yamamoto, T. (2003). *Nucl. Instrum. Methods Phys. Res. A*, **508**, 425–433.
Knoll, G. F. (2000). *Radiation Detection and Measurement*, 3rd ed. New York: John Wiley & Sons.
Laundy, D., Tang, C., Roberts, M., Miller, M., Thompson, S. & Bushnell-Wye, G. (2003). *J. Synchrotron Rad.* **10**, 183–186.
MacLean, E. J., Millington, H. F. F., Neild, A. A. & Tang, C. C. (2000). *Mater. Sci. Forum*, **321–324**, 212–217.
Tang, C. C., Thompson, S. P., Hill, T. P., Wilkin, G. R. & Wagner, U. H. (2008). *Z. Kristallogr.* Accepted.